PHYSICALLY-BASED DEFORMABLE IMAGE REGISTRATION WITH MATERIAL PROPERTY AND BOUNDARY CONDITION ESTIMATION

Huai-Ping Lee[1]*, Mark Foskey*[1,2]*, Marc Niethammer*[1]*, and Ming Lin*[1]

[1]Department of Computer Science, [2]Department of Radiation Oncology,
University of North Carolina, Chapel Hill, NC, USA

ABSTRACT

We propose a new deformable medical image registration method that uses a physically-based simulator and an iterative optimizer to estimate the simulation parameters determining the deformation field between the two images. Although a simulation-based registration method can enforce physical constraints exactly and considers different material properties, it requires hand adjustment of material properties, and boundary conditions cannot be acquired directly from the images. We treat the material properties and boundary conditions as parameters for the optimizer, and integrate the physically-based simulation into the optimization loop to generate a physically accurate deformation automatically.

Index Terms— Non-rigid image registration, physically-based simulation

1. INTRODUCTION

Image registration has become an integral part of image-guided radiotherapy. In order to estimate the radiation dose accumulated in different parts of the tissue, it is important to find out the correspondence relating each pixel from each image taken during treatment to its corresponding pixel in the reference image, which is usually taken before the treatment. Given the reference image I_f and a moving image I_m, the goal of a deformable registration is to find a deformation field that maps each pixel of I_m to a pixel in I_f. Traditionally, the registration is formulated as an optimization problem with the discrete deformation field as the parameters, and some error metric based on image similarity is minimized [1]. To cope with the high dimensionality of the problem, some regularization terms based on smoothness of the deformation or physically-based energy can be added to the objective function to be minimized [2]. Alternatively, the objective function can be assessed only on some landmarks, with the deformation field interpolated for the entire domain using appropriate basis functions [3].

Another type of method generates the deformation using a physically-based simulation [4], given the segmented organs in the moving image. Methods of this type enforce physical constraints exactly and take different material properties into account, unlike the optimization-based methods, where the image similarity and the regularization terms need to be carefully balanced, and the entire domain is modeled as one material. However, the boundary conditions (deformation vectors or external forces on some boundary locations) and material properties (stiffness and compressibility) for the simulation need to be chosen to achieve the desired shapes in the reference image. When both images are segmented, boundary conditions can be approximated with surface matching methods, but there is no guarantee of quality and physical accuracy in such a matching. The material properties are usually adjusted by hand and can be different for each patient. A recent work [5] uses an optimizer to find out the material properties and boundary forces for a 2D image registration problem, but it is only implemented on 2D images with a low resolution model.

Our method is inspired by *ultrasound elastography* [6], which is a non-invasive method for cancer detection, based on the assumption that cancerous tissues tend to be stiffer than normal ones. Elastography is done by first estimating the deformation of each pixel by, in effect, comparing two ultrasound images, one taken at rest state and the other taken when a known force is imposed. After that, the elasticities can be computed by solving a least-squares problem or by minimizing errors in deformation field iteratively. Although the image registration problem also estimates the deformation field that maps one image to another, there are fundamental differences. First, elastography is done at the tissue level, while the image registration is done at the multi-organ level. Moreover, the external forces are unknown in image registration, and the deformation field cannot be obtained directly from the images. For this reason, our method uses an iterative optimization framework to estimate the deformation and simulation parameters (elasticity and boundary conditions) at the same time. In each optimization loop, a deformation field is generated by the physically-based simulator with the current set of parameters. An objective function based on the registration error when applying the deformation field is minimized by updating the simulation parameters for the next iteration. We measure registration error based on correspondence at the boundaries of segmented organs, but a variety of measures could be applied. In addition to matching the organ boundaries, the deformation generated by our method is always the

result of a 3D physically-based simulation, therefore quality and physical accuracy are enforced.

2. METHOD

The inputs to the algorithm are two segmented images, the reference image I_f with segmentation $\mathbf{S}_f$, and the moving image I_m with segmentation $\mathbf{S}_m$. We assume the bones are already aligned by a rigid transformation. Our goal is to find a deformation field $\mathbf{u}$ that maps the moving image I_m to the reference image I_f. Each segmentation is represented as a set of closed triangulated surfaces, one for each segmented object. To numerically solve the constitutive equations of elasticity, we construct a tetrahedralization of the moving image such that each face of $\mathbf{S}_m$ is a face in the tetrahedralization, so that $\mathbf{S}_m$ is characterized entirely by its set of nodes. Our algorithm uses a quasi-Newton optimizer [7] to minimize an objective function based on the registration error, and each evaluation of the function and its gradient is essentially a simulation using the current set of parameters $\mathbf{x} = [\mathbf{E}; \mathbf{F}]^T$, which consists of the material properties $\mathbf{E}$ (we consider only the Young's modulus in this paper) and boundary forces $\mathbf{F}$. In this section we briefly present our algorithm. Interested readers are referred to [8] for more details.

2.1. Linear elasticity model and finite element modeling

The basis of our algorithm is a physically-based simulator that generates deformation field. Currently, we use the linear elasticity model solved with the finite element method, as described in [4]. Assuming linear elasticity, the stress vector $\sigma = [\sigma_x, \sigma_y, \sigma_z, \tau_{xy}, \tau_{yz}, \tau_{xz}]^T$ is a linear transformation of the strain vector ϵ (change of shape or size), and the transformation is defined by the material properties (assuming an isotropic material, the properties are Young's modulus and Poisson's ratio) of the elastic body. The strain vector is defined by the derivatives of the deformation $\mathbf{u} = [u, v, w]^T$:

$$\epsilon = \left[\frac{\partial u}{\partial x}, \frac{\partial v}{\partial y}, \frac{\partial w}{\partial z}, \frac{\partial u}{\partial y} + \frac{\partial v}{\partial x}, \frac{\partial v}{\partial z} + \frac{\partial w}{\partial y}, \frac{\partial u}{\partial z} + \frac{\partial w}{\partial x}\right]^T = \mathbf{L}\mathbf{u}, \tag{1}$$

and the simulation essentially amounts to solving the constitutive equation for the deformation $\mathbf{u}$, given the external forces $[f_x, f_y, f_z]^T$:

$$\begin{aligned} \frac{\partial \sigma_x}{\partial x} + \frac{\partial \tau_{xy}}{\partial y} + \frac{\partial \tau_{xz}}{\partial z} + f_x &= 0 \\ \frac{\partial \tau_{xy}}{\partial x} + \frac{\partial \sigma_y}{\partial y} + \frac{\partial \tau_{yz}}{\partial z} + f_y &= 0 \\ \frac{\partial \tau_{xz}}{\partial x} + \frac{\partial \tau_{yz}}{\partial y} + \frac{\partial \sigma_z}{\partial z} + f_z &= 0. \end{aligned} \tag{2}$$

We solve Eq. 2 numerically using the finite element method (FEM), which is based on the discretization of the domain into a finite number of elements, with each element consisting of several nodes. We use tetrahedra as elements, so that each consists of four nodes. The deformation field within an element is approximated by a linear function, based on the nodal deformation vectors $\mathbf{u}_j^{el}$ $(j = 1, 2, 3, 4)$,

$$\hat{\mathbf{u}}^{el}(\mathbf{p}) = \sum_{j=1}^{4} \mathbf{u}_j^{el} N_j^{el}(\mathbf{p}), \tag{3}$$

where N_j^{el} is the linear shape function that has value one at the j-th node and zero at other nodes. The result of combining the linear shape functions for each element is a global linear system

$$\mathbf{K}\mathbf{u} = \mathbf{F}, \tag{4}$$

where $\mathbf{K}$ is the *stiffness matrix*, which contains the information of geometry and material properties, and $\mathbf{F}$ is the vector consisting of external forces on each node, which is zero except at nodes with boundary conditions assigned.

2.2. Objective function

The objective function is defined as the distance between the deformed moving surface $\mathbf{S}_m$ and the reference surface $\mathbf{S}_f$,

$$\Phi(\mathbf{x}) = \frac{1}{2} \sum_{\mathbf{v}_l \in \mathbf{S}_m} \left\| \mathbf{d}\left(\mathbf{v}_l + \mathbf{u}_l(\mathbf{x}), \mathbf{S}_f\right) \right\|^2, \tag{5}$$

where $\mathbf{u}(\mathbf{x})$ is the deformation field computed by the simulator with parameters $\mathbf{x}$, interpreted as a displacement vector for each node $\mathbf{v}_l$ in the tetrahedralization. The notation $\mathbf{d}(\mathbf{v}, \mathbf{S})$ denotes the shortest distance vector from the surface $\mathbf{S}$ to the node $\mathbf{v}$, and the sum is taken over all nodes of the moving surface. In practice, the distance can be looked up in a precomputed distance map of the reference surface $\mathbf{S}_f$. The distance vectors at the boundary nodes can also serve as the initial guess for boundary conditions of the first kind (i.e., assigned displacement vectors), and the initial forces can be computed from these boundary conditions and an initial guess of elasticities via Eq. 4.

The gradient of the objective function is given by the chain rule,

$$\nabla\Phi(\mathbf{x}) = \sum_{\mathbf{v}_l \in \mathbf{S}_m} \mathbf{J}^T \left[\frac{\partial \mathbf{d}\left(\mathbf{v}_l + \mathbf{u}_l, \mathbf{S}_f\right)}{\partial \mathbf{u}}\right] \mathbf{d}\left(\mathbf{v}_l + \mathbf{u}_l(\mathbf{x}), \mathbf{S}_f\right) \tag{6}$$

where $\mathbf{J} = \left[\frac{\partial u_i}{\partial x_j}\right]$ is the Jacobian matrix of $\mathbf{u}(\mathbf{x})$. Here we use the bracket $[\cdot]$ to represent a matrix and the curly braces $\{\cdot\}$ to denote a vector. Each row of the matrix, $\left[\frac{\partial \mathbf{d}(\mathbf{v}_l + \mathbf{u}_l, \mathbf{S}_f)}{\partial u_j}\right]$, is essentially the spatial derivative of $\mathbf{d}\left(\mathbf{v}_l + \mathbf{u}_l, \mathbf{S}_f\right)$ with respect to the j-th axis. The derivatives of $\mathbf{u}$ with respect to the elasticities are computed by differentiating both sides of Eq. 4,

$$\left[\frac{\partial \mathbf{K}}{\partial E_j}\right] \mathbf{u} + \mathbf{K} \left\{\frac{\partial \mathbf{u}}{\partial E_j}\right\} = 0, \tag{7}$$

and therefore the Jacobian matrix can be computed by solving $\mathbf{K}\left\{\frac{\partial \mathbf{u}}{\partial E_j}\right\} = \left[\frac{\partial \mathbf{K}}{\partial E_j}\right]\mathbf{u}$ for each column $\mathbf{J}_j$. Similarly, the derivatives of $\mathbf{u}$ with respect to the forces can be computed by differentiating both sides of Eq. 4,

$$\left[\frac{\partial \mathbf{K}}{\partial F_j}\right]\mathbf{u} + \mathbf{K}\left\{\frac{\partial \mathbf{u}}{\partial F_j}\right\} = \mathbf{e}_j, \tag{8}$$

where $\mathbf{e}_j$ is the j-th coordinate vector. Since the matrix $\mathbf{K}$ is independent of the forces, we have $\mathbf{K}\mathbf{J}_j = \mathbf{e}_j$. Notice that the optimization framework can work with different physical models or numerical solvers, as long as the derivatives $[\partial \mathbf{u}/\partial \mathbf{x}]$ can be computed.

In practice, the gradient of Φ is much smaller with respect to $\mathbf{E}$ than with respect to $\mathbf{F}$, which causes the elasticity to converge very slowly. To accelerate the process, we use an alternating approach: we optimize the forces while keeping the elasticities constant for n steps, and then use the resulting forces to optimize the elasticities for n steps, and then go back to optimizing the forces, and so on. In our experiments, n is set to five.

2.3. Numerical optimization

We adopt a line search scheme to minimize the objective function Φ: At the k-th iteration, a descent direction $\mathbf{p}_k$ is computed based on the gradient of Φ, and we search for an optimal step size λ_k along the direction based on the value and slope of the function $\Phi(\lambda) = \Phi(\mathbf{x}_k + \lambda \mathbf{p}_k)$, where $\mathbf{x}_k$ is the current estimate of the parameters. The Newton's method uses the Hessian matrix to find the descent direction and has a quadratic convergence rate. However, the Hessian is hard to compute or even ill-conditioned in many cases. Therefore, we use a quasi-Newton method (the limited memory BFGS method), which uses the history of the gradient in previous steps to estimate the curvature and compute a symmetric positive definite approximation of the Hessian matrix [7]. The quasi-Newton method saves computation time for computing the Hessian matrix while maintaining a super-linear convergence rate.

3. EXPERIMENTS

We applied our method to three pairs of CT images of the male pelvis, each pair taken from a different patient. The resulting RMS errors in the segmentation boundaries for the three pairs of images are 0.076 cm, 0.065 cm, and 0.081 cm, respectively, which are within the image resolution (0.1x0.1x0.3 cm for the first two pairs of images and 0.12x0.12x0.15 cm for the third pair). One of the moving images before and after applying our registration algorithm is shown in Fig. 1. Notice how the organs fit the segmentation boundaries after the registration. The image intensity, however, provides little information inside the organs since

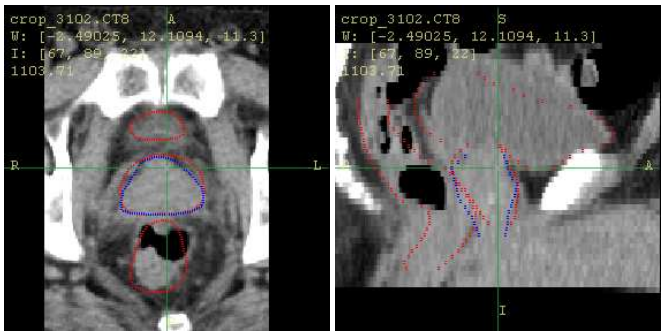

(a)

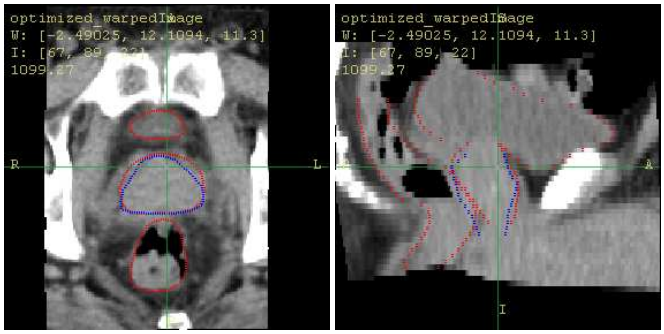

(b)

Fig. 1: The axial and sagittal views of the moving image (a) before and (b) after the registration using our method. The red contours show the organ boundaries of the reference image, and the blue contours show the boundary of the prostate in the moving image. Notice how the organs move towards the red contour.

the intensity is nearly constant inside. In order to validate the correctness of the resulting deformation field, we picked those images with bright spots in the prostate due to accumulated calcium. The bright spots serve as landmarks inside the prostate and can provide more information about the deformation inside the organ. The resulting errors in landmark positions are compared against the results of a rigid registration and two other non-rigid registration methods: the Demons method [1] and the B-spline registration method [2]. The Demons method is based on local intensity differences and gradients, so it has an advantage due to the high intensity and contrast of the landmarks, while our method relies on the segmentations and does not use any information in image intensities. We avoid such an advantage by replacing the prostate with its the label map: a single intensity value (the average intensity inside the organ) is assigned to the pixels occupied by the organ. The B-spline method uses B-splines to model the free-form deformation to ensure that the transformation is diffeomorphic (smooth and invertible), and therefore the accuracy in the organ boundaries is sometimes compromised. The resulting errors in landmark position are shown in Table 1. The results show that while all three methods can generate low registration error in terms of image intensity, the quality of the deformation varies. Our method generates the deformation field using a physically-

		Rigid Transformation	Demons (label map of prostate)	B-Spline Registration	Our Method
Patient 1	Landmark 1	0.5594	0.3449	0.3525	0.1971
	Landmark 2	0.5580	0.3795	0.3295	0.2830
	Landmark 3	0.5180	0.2577	0.3299	0.2294
	Landmark 4	0.3585	0.2993	0.2099	0.0513
	Average	0.4985	0.3204	0.3146	0.1902
Patient 2	Landmark 1	0.3336	0.1753	0.3054	0.2773
Patient 3	Landmark 1	0.2376	0.3045	0.2728	0.2198
	Landmark 2	0.4000	0.2723	0.3801	0.2337
	Landmark 3	0.4081	0.4264	0.3720	0.3411
	Landmark 4	0.2350	0.3036	0.2708	0.2607
	Landmark 5	0.1120	0.1556	0.1690	0.2215
	Average	0.2785	0.2925	0.2929	0.2554
All Patients	Average	0.3720	0.2919	0.3025	0.2315

Table 1: Error of landmark positions (distance in cm) inside the prostate

based simulation, therefore the quality of the deformation can be guaranteed, and the errors in landmark position are the lowest overall.

4. CONCLUSIONS

We have presented a physically-based image registration method that automatically determines material properties and boundary conditions. Compared to traditional optimization-based methods which minimizes image metrics and regularization terms, our method does not require a trade-off between image similarity and the quality of the deformation, since our deformation field is always generated by a physically-based simulation. Our method not only matches the segmentation boundaries, but also generates high-quality deformations inside the organs. Our framework is general and can be modified to use different physical models easily. Furthermore, our method does not require any tedious process of parameter adjustment and is automatic once the segmentation of both the moving and the reference images are given.

Since our method depends on the segmentation of the images, the resulting elasticity values may differ while the registration error remains low. In the future, we would like to investigate the effect of segmentation error on the optimal parameters and incorporate other image- or landmark-based metrics to further reduce the burden and possible error from the hand segmentation. We would also like to apply the framework to more complicated geometric and physical models to improve the accuracy of registration.

5. REFERENCES

[1] J.-P. Thirion, "Image matching as a diffusion process: an analogy with maxwell's demons," *Medical Image Analysis*, vol. 2, no. 3, pp. 243–260, 1998.

[2] M. Holden, "A review of geometric transformations for nonrigid body registration," *Medical Imaging, IEEE Transactions on*, vol. 27, no. 1, pp. 111–128, 2008.

[3] K. Rohr, H.S. Stiehl, R. Sprengel, T.M. Buzug, J. Weese, and M.H. Kuhn, "Landmark-based elastic registration using approximating thin-plate splines," *Medical Imaging, IEEE Transactions on*, vol. 20, no. 6, pp. 526–534, June 2001.

[4] J. M. Hensel, C. Menard, P. W. M. Chung, M. F. Milosevic, A. Kirilova, J. L. Moseley, M. A. Haider, and K. K. Brock, "Development of multiorgan finite element-based prostate deformation model enabling registration of endorectal coil magnetic resonance imaging for radiotherapy planning," *Int. J. Radiation Oncology Bio. Phys.*, vol. 68, no. 5, pp. 1522–1528, 2007.

[5] R Alterovitz, K Goldberg, J Pouliot, ICJ Hsu, Y Kim, SM Noworolski, and J Kurhanewicz, "Registration of MR prostate images with biomechanical modeling and nonlinear parameter estimation," *Medical Physics*, vol. 33, pp. 446, 2006.

[6] F Kallel and M Bertrand, "Tissue elasticity reconstruction using linear perturbation method," *Medical Imaging, IEEE Transactions on*, vol. 15, no. 3, pp. 299–313, 1996.

[7] J Nocedal and SJ Wright, *Numerical Optimization*, Springer, 1999.

[8] H.-P. Lee, M. Foskey, M. Niethammer, and M. C. Lin, "Simulation-based joint estimation of body deformation and elasticity parameters," Tech. Rep. TR09-014, University of North Carolina-Chapel Hill, 2009.